A Novel Approach to the Interpretation and Prediction of Solvent Effects in the Synthesis of Macroporous Polymers

Stefan Scheler

Department of Pharmaceutical Technology, Friedrich Schiller University Jena, Lessingstrasse 8, 07743 Jena, Germany

Received 15 May 2006; accepted 5 March 2007
DOI 10.1002/app.26431
Published online 23 May 2007 in Wiley InterScience (www.interscience.wiley.com).

ABSTRACT: A trivariate interpolation technique, the modified Shepard's method, was applied for the first time to explain and predict various properties of macroporous polymers from the Hansen solubility parameters of the porogens employed for polymerization. Highly crosslinked polymers and copolymers were prepared from ethylene glycol dimethacrylate and methacrylic acid by free-radical polymerization with 30 different porogenic solvents. Instead of the spherical model used by Hansen, detailed three-dimensional maps were computed to represent the measured properties in a δ_d–δ_p–δ_h diagram (where δ_d, δ_p, and δ_h are the Hansen solubility parameters according to the three types of bonding forces: dispersion, polar, and hydrogen-bonding, respectively). This method was able to detect unapparent correlations between the different polymer properties, thus providing a better understanding of the pore-formation process. An important finding was the crucial role of the initiator solubility and its partitioning between the solution and the polymer surface, which proved to be key factors for the explanation of many contradictory solvent effects. © 2007 Wiley Periodicals, Inc. J Appl Polym Sci 105: 3121–3131, 2007

Key words: macroporous polymers; phase separation; swelling

INTRODUCTION

Macroporous polymers have found widespread use in many technical and medical applications, such as ion exchangers, adsorbents, chromatographic packing, polymeric reagents, supports for heterogeneous catalysis or solid-phase synthesis,[1] and scaffolds for the growth of mammalian cell cultures or the production of biomass.[2] Because of the tremendous growth of such fields as combinatorial chemistry, solid phase catalysis, and separation science, research on these kinds of materials has experienced a considerable uptrend in the past years.[3] Macroporous polymers can be produced as spherical beads by suspension polymerization or in the form of monoliths prepared by polymerization within the confines of an unstirred mold, but other forms such as macroporous membranes have also been reported. Regardless of their preparation mode, they are characterized by a permanent porosity that persists even in the dry state. The structure of macroporous polymers is formed by interconnected globules (10–50 nm) that are partly aggregated in larger clusters. The pores consist of irregular voids located between these clusters (macropores) or between the globules of a given cluster (mesopores and micropores). This typical morphology is generated by phase separation, which occurs if polymerization takes place in a liquid phase (porogen) that is a nonsolvent for the formed polymer. Different applications of macroporous polymers require individual designs and tailored pore size distributions. Although the mechanism of pore formation that occurs during the polymerization process has been reviewed several times, the knowledge about factors controlling the pore size was mostly empirical for many years.[4–8] In recent decades, some authors have developed kinetic and thermodynamic models for the description of the structure-formation process.[9,10] Okay[10] correlated the total porosity of macroporous styrene/divinyl benzene copolymer networks with the Hildebrand solubility parameters of the diluent and polymer, with the degree of crosslinking, and with the monomer dilution. Malik et al.[11] developed regression equations to predict the estimated pore volume of porous styrene/divinyl benzene copolymer beads from the Hildebrand solubility parameters, weight fractions of the monomers, and diluent.[11] Furthermore, they estimated the pore size distribution, the surface area, and the swelling coefficient in acetone on the basis of the polymer bead density in the dry state.[12]

The most effective parameters influencing the pore size distribution are the concentrations of monomers and free-radical initiator, the reaction temperature, and, in particular, the type of porogen. The solvent

Correspondence to: S. Scheler (stefan.scheler@uni-jena.de).

effects have been especially investigated by many authors, but they are often contradicting. Some authors have discussed the influence of the molecule size of the porogen,[13] but more commonly its solubility or ability to swell a polymer is considered to play the major role in pore formation. Several investigators have simply compared the opposite effects of lipophilic and hydrophilic diluents and their mixtures on the polymer structure, whereas others have characterized the solvent properties by their alkyl chain lengths.[14–16] A more exact concept is the application of Hildebrand's solubility parameters, but even this cannot explain all observed effects.[17,18] Those single parameter correlations have the disadvantage of a more limited prediction potential than that of multiparameter approaches.[8,19] Several workers have therefore proposed two-, three-, four-, or even five-dimensional scales. Among the most successful has been Hansen's three-dimensional solubility parameter. In Hansen's scheme, the total Hildebrand value is subdivided into three fractions: a dispersion-force component, a hydrogen-bonding component, and a polar component, which are usually visualized in a three-dimensional coordinate system. However, this method suffers from the graphic difficulty of displaying the dependent variable as a fourth dimension in the space and from the resulting interpretation complexity.[20]

The aim of this investigation was to overcome these problems by the application of a sophisticated computer-aided data visualization technique. It should allow precise predictions of material properties for polymers prepared with any kind of porogen or porogen mixture on the basis of a preliminary dataset obtained with a limited number of standard solvents. Another goal was to improve our knowledge of the pore-formation process.

EXPERIMENTAL

Preparation of the porous polymers

Sixty macroporous polymer samples were prepared with 30 different porogens and two monomer formulations. The first was a mixture consisting of 6 mmol of ethylene glycol dimethacrylate (EDMA; Merck, Darmstadt, Germany), 0.07 mmol of azobisisobutyronitrile (AIBN; Acros Organics, Geel, Belgium), and 1.5 mL of a porogen. The second contained 5 mmol of EDMA, 1 mmol of methacrylic acid (MAA; Merck), 0.07 mmol of AIBN, and 1.5 mL of a porogen. All mixtures were prepared in 8-mL glass vials that were sealed with rubber stoppers and metal caps after being filled and purged with nitrogen. Polymerization was carried out for 24 h in a water bath at 60°C. After the vials were broken, the formed polymer cylinders were removed and vacuum-dried at 25°C and a pressure of 5 Pa. In the case of nonvolatile porogens, the samples were washed with methanol five times before drying.

Preparation of the nonporous polymer plates

Polymer plates for the determination of the swelling properties were cast from solvent-free monomer mixtures in Petri dishes. The dishes were placed in an desiccator, flushed with nitrogen, and polymerized for 24 h in a hot-air cabinet at 60°C.

Determination of the swelling properties

The affinity of each solvent for the two polymers was estimated by the swelling degree of the nonporous polymer plates. Fragments of the polymer plates were prepared, and their thickness was measured with a micrometer screw before and after 24 h of incubation at 20°C. The swelling was calculated as the ratio of the thicknesses after and before incubation. For each solvent, the swelling ratio was determined three times.

Determination of the specific surface area

For the determination of the surface area by nitrogen adsorption [the Brunauer–Emmett–Teller (BET) method], porous polymer samples were crushed in a mortar and ground to obtain a sieve fraction between 0.5 and 1.4 mm. The BET surface was determined by an SA 3100 surface analyzer (Beckman Coulter, Inc., Fullerton, CA).

Solubility of AIBN in different solvents

A solvent (1 mL) was added to 200 mg of AIBN and was shaken for 2 h at room temperature. The mixture was observed visually for an undissolved substance and then filtered through a 0.2-μm polytetrafluoroethylene membrane. The solvent was removed from the filtrate by vacuum drying for 3 days at 20°C and a pressure of 9 Pa. Because AIBN partially sublimates under these conditions, a gravimetrical analysis was not feasible. For this reason, the solubility was estimated by visual observation and specified as a score on a rating scale ranging from 0 to 1. The classification was performed with the criteria ''unsolved substance after 2 h of shaking with the respective solvent'' and ''residue after 3 days of vacuum drying'' as follows: 0, remaining unsolved substance, no residue after drying; 0.25, remaining unsolved substance, small residue after drying; 0.5, remaining unsolved substance, residue after drying; 0.75, remaining unsolved substance, large residue after drying; and 1, no remaining unsolved substance, large residue after drying.

TABLE I
Properties of the Tested Polymer Samples

	Porogen	Swelling (%)		Surface area (m^2/g)		Solubility of AIBN (score)	C=C/C=O IR absorbance ratio for poly (EDMA-*co*-MAA)
		Poly (EDMA-*co*-MAA)	Poly EDMA	Poly (EDMA-*co*-MAA)	Poly EDMA		
1	Acetone	2.03	0.49	299.9	402.6	1	46.6
2	Acetonitrile	1.92	1.20	312.5	385.4	1	26.0
3	Acetophenone	2.28	0.28	340.5	387.2	0.75	19.4
4	Benzyl alcohol	1.18	0.85	320.4	401.3	0	47.8
5	*n*-Butanol	1.42	0.38	233.3	232.4	0	22.4
6	*n*-Butyl acetate	0.64	0.52	353.0	427.7	0	22.0
7	Chloroform	1.69	2.62	267.6	281.8	1	25.2
8	Cyclohexane	0.73	0.18	5.9	17.6	0	22.5
9	Cyclohexanol	0.60	0.59	350.7	387.9	0	19.7
10	1,4-Dioxane	1.30	0.72	253.7	369.8	1	23.1
11	Dimethylformamide	2.10	0.52	381.4	488.8	1	9.9
12	Dimethyl sulfoxide	1.93	0.52	326.0	421.1	0.75	22.9
13	Ethanol	1.77	0.88	196.9	170.1	0.25	21.9
14	Ethyl acetate	1.87	1.21	347.9	441.5	0	24.4
15	Ethylene glycol	0.71	0.59	—	—	—	—
16	Hexane	0.68	0.41	4.0	6.0	0	28.0
17	Methanol	2.70	2.22	105.2	91.4	0.25	20.4
18	2-Methoxyethanol	1.32	0.92	372.8	480.3	0.5	16.4
19	Methyl acetate	2.31	2.30	304.3	413.1	1	32.1
20	Methylene chloride	4.25	5.03	251.0	275.9	1	25.2
21	Methyl ethyl ketone	2.76	1.70	367.1	454.7	1	20.8
22	Methyl isobutyl ketone	0.72	0.44	351.7	431.8	0.25	26.6
23	1-Propanol	1.56	0.35	237.5	264.0	0	22.4
24	2-Propanol	1.12	0.74	237.0	258.9	0	18.6
25	Propylene glycol	0.91	0.53	37.8	54.6	0	29.9
26	Pyridine	2.07	1.08	91.2	326.1	1	24.3
27	Tetrahydrofuran	0.82	0.71	369.3	518.4	1	17.5
28	Tetrahydrofurfuryl alcohol	1.29	0.60	454.2	575.3	1	24.9
29	Toluene	0.95	0.97	325.4	443.2	0	22.8
30	Xylene	3.18	0.74	243.4	411.6	0	24.7

IR spectra of unreacted vinyl groups

The IR absorption of poly(EDMA-*co*-MAA) (KBr pellet, 100:1 ratio of KBr to the sample powder) was measured with a Nicolet Avatar 370 DTGS Fourier transform infrared spectrometer (Thermo Electron Corp., Waltham, MA). To obtain a nominal value for the relative concentrations of the unpolymerized double bonds in each polymer sample, the absorbance ratios were calculated from the C=C stretch vibration (ca. 1636 cm^{-1}) and the C=O vibration of the carboxyl group (ca. 1730 cm^{-1}). The carboxyl group of MAA had a constant concentration in all samples and therefore could be used to normalize the double-bond signal.

RESULTS AND DISCUSSION

Polymerization process

Table I gives an overview of the experimental results, which are subsequently discussed.

The mechanism of pore formation depends mainly on the type of porogen used for the creation of the porous structure. The organic phase contains monovinyl and divinyl monomers (in the case of polyEDMA, only divinyl monomers), an initiator, and a porogenic solvent. At the reaction temperature of 60°C, the free-radical initiator is decomposed, and the initiating radicals start the polymerization process in solution. The growing polymers precipitate after they become insoluble in the reaction medium as a result of crosslinking. The critical chain length for the growing polymer to become insoluble is smaller in poor solvents and higher in good solvents for the polymer; this results in smaller primary particles if the solubility is low. If the monomers are thermodynamically better solvating agents for the polymer than the porogen, the precipitated nuclei are swollen with the monomers. Polymerization within the swollen nuclei is kinetically preferred because the local concentration of monomers is higher there than in the surrounding solution. Contrary to the first step of particle formation, in this stage of the process, porogens with low solubility for the polymer are accounting for larger particles. However, in the dispersion polymerization of highly crosslinked polymers, the swelling, if it occurs at all,

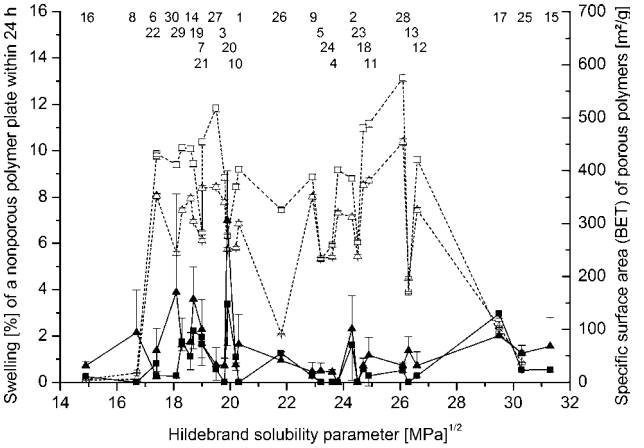

Figure 1 (—) Swelling degree of nonporous polymer plates and (· · ·) specific surface area of porous polymer samples versus the Hildebrand solubility parameter: (▲, △) poly(EDMA-*co*-MAA) and (■, □) polyEDMA. See Table I for an explanation of the solvent numbers.

is confined to the surface layers of the primary particles because of their rigid structure. Instead, particle growth is achieved mainly by the precipitation of nucleated oligomers onto the surface of the nuclei.[21,22] In the third stage, more or less enlarged nuclei associate in clusters being held together by polymer chains that crosslink the neighboring particles. It can be assumed that this aggregation process is promoted by porogens with a low affinity to the polymer. When the size of the clusters becomes large enough to allow mutual contact, a scaffolding-like interconnected matrix is formed.

As discussed, the influence of the porogen becomes manifest in three different stages of the reaction sequence leading to opposite effects on the particle size. This fact complicates the correlation between the porogen properties and the resulting polymer structure. The size distribution of the matrix-forming globules is not readily accessible by direct measurement, but the specific surface area of the polymer can be considered to be closely related to the size of the globular subunits and their degree of fusion.[17] Both polymers investigated are totally insoluble in any solvent because of their high degree of crosslinking, but the swelling behavior of nonporous polymer samples prepared by bulk polymerization allows an estimation of their affinities to different solvents. The swelling of a polymer in a liquid is maximum when the solubility parameters of the solvent and polymer match. In the case of polymers with more than one type of functional group or copolymers, even more than one maximum may be observed, but in practice, the variation in the polar and hydrogen-bonding properties of both the polymer and liquids causes considerable scatter in many of these plots.[23] For both polymers examined in this work, the swelling degree of the nonporous samples does not show any correlation to various parameters of the incubation medium, such as the permittivity or Hildebrand solubility parameter. Also, the specific surface of the porous samples does not correlate with the aforementioned parameters of the porogens employed for the preparation (Fig. 1).

Solubility parameters

Hildebrand and Scott[24] originally defined the solubility parameter (δ) of a substance as the square root of the cohesive energy density, which is a direct reflection of the degree of cohesive forces holding the molecules together:

$$\delta = \sqrt{\frac{\Delta H - RT}{V_m}} \tag{1}$$

where ΔH is the heat of vaporization, R is the gas constant, T is the temperature, and V_m is the molar volume.

Hansen[25] extended the solubility parameter concept by subdividing the cohesive energy (E_{coh}) into three fractions corresponding to the London dispersion forces, Keesom dipolar forces, and hydrogen bonding:

$$E_{coh} = E_d + E_p + E_h \tag{2}$$

where E_d, E_p, and E_h are the contributions of dispersion, polar, and hydrogen-bonding forces, respec-

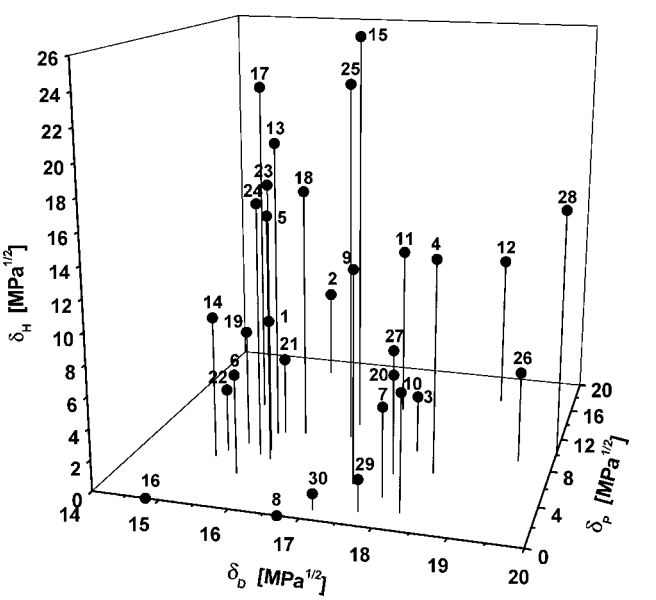

Figure 2 Positions of the tested solvents within a δ_d–δ_p–δ_h diagram. See Table I for an explanation of the solvent numbers.

tively. The corresponding equation for the total solubility parameter (δ_t) is

$$\delta_t^2 = \delta_d^2 + \delta_p^2 + \delta_h^2 \quad (3)$$

where δ_d, δ_p, and δ_h are the Hansen solubility parameters according to the three types of bonding forces. δ_t can be plotted as a vector in a three-dimensional δ_d–δ_p–δ_h space. The length of δ_t is equal to Hildebrand's one-dimensional parameter δ. Figure 2 shows the positions of the 30 tested solvents within a three-dimensional diagram.

Hansen calculated the cohesion parameters of a polymer as the center of a sphere enclosing all solvents in which the polymer is soluble or swellable (the latter in the case of crosslinked polymers). Instead of spherical shapes, Beerbower and Dickey[26] considered constant percentage swelling contours as rectangular boxes. For a quantitative estimate of the swelling, a series of concentric boxes can be drawn for each polymer, with copolymers having two families of concentric boxes. The visualization of the solubility region of a given polymer or the functional dependence of other polymer properties on Hansen parameters requires plotting a dependent variable versus three independent variables (δ_d, δ_p, and δ_h). The four-dimensional data of this type cannot be visualized in orthogonal projections,[27,28] two-dimensional contour plots, or projections of three-dimensional contour surfaces[29,30] without any loss of valuable information. This applies also to all methods that combine two of the three Hansen parameters to a new variable[31,32] and to the triangular plot proposed by Teas[33] in which the loss of information is due to a normalization of the Hansen parameters by their sum. In this case, the solubility behavior is determined, not by differences in the total Hildebrand value, but by the relative amounts of the three Hansen parameters, which results in poorly defined solubility regions, with many solvents scattered among nonsolvents. Although it is widely used, there is no theoretical justification for this plotting technique.[34] Another method for the illustration of four-dimensional datasets was proposed by Van de Mark and Lian,[20] who depicted the degree of polymer swelling as the size of cubic markers centered at each solvent's position in the three-dimensional coordinate system defined by Hansen parameters. A similar approach of plotting single data points instead of calculated contours, chosen by Wernick,[19] is to compute three-dimensional plots as stereopairs providing spatial impressions. Because the levels of dependent variables, such as the solubility, are displayed by different symbol shapes, a ready perception of those graphics is difficult.

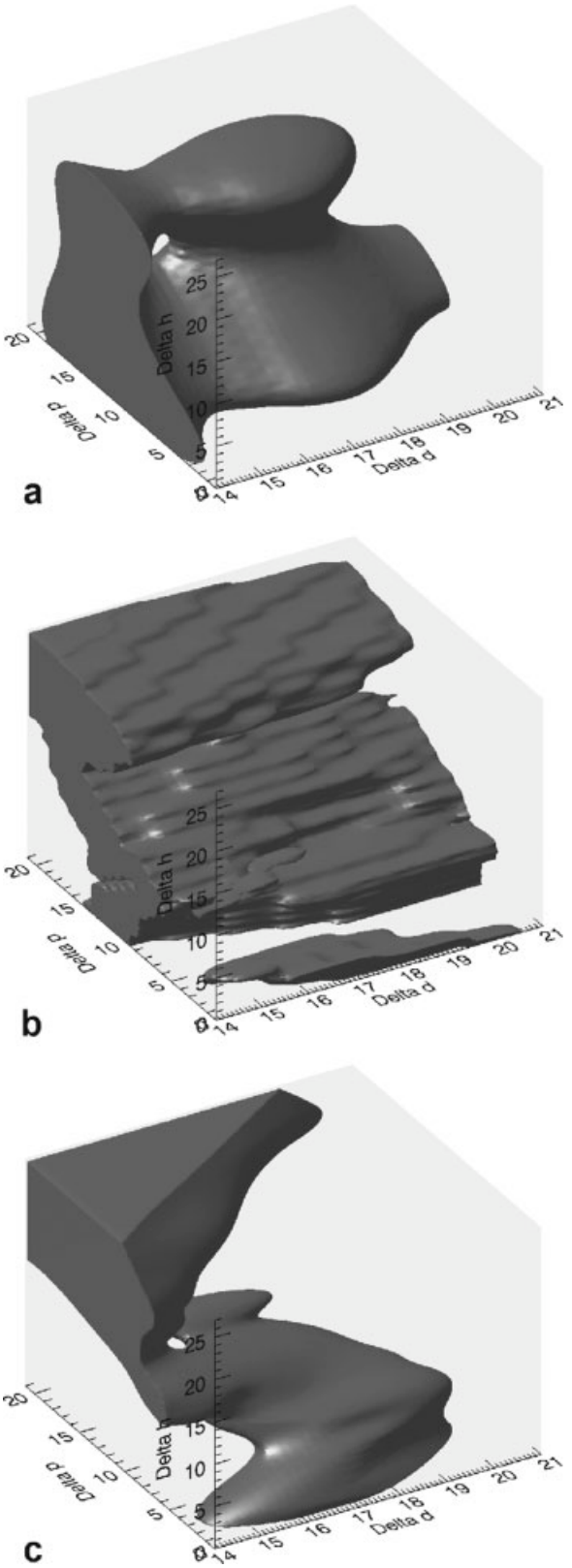

Figure 3 Three-dimensional representation of poly(EDMA-*co*-MAA) swelling in terms of the Hansen parameters ($MPa^{1/2}$). The interval volume encloses all the solvents causing polymer swelling greater than or equal to 2%: (a) computation by multiple polynomial regression, (b) computation by the nearest neighbor method, and (c) computation by the modified Shepard's method.

Calculation of the interval volumes

A novel approach was used in this work. The regions of swellability in the δ_d–δ_p–δ_h diagram were

calculated in more detail as an interpolated density distribution and were depicted as a three-dimensional volume surrounded by an isosurface. This allowed precise cartography of the whole diagram space. A similar strategy was reported by Crowley et al.,[29,30] who assigned the Hildebrand solubility parameter, dipole moment, and hydrogen bonding to the *X*, *Y*, and *Z* axes, respectively. On the basis of three-dimensional models constructed with colored balls and glass rods, resembling Figure 2, spatial contour drawings were sketched. Because of their manual creation, those graphics are only coarse mappings unsuitable for precise graphic analyses. In this work, however, recent mathematical algorithms were used for the computation of exactly defined spatial distributions. The calculations were done by data gridding and subsequent interval volume tetrahedrization[35] using the software packages IDL 6.0 (Research Systems, Inc., Boulder, CO) and MATLAB 7.0.4 (MathWorks, Inc., Natick, MA). Two different interpolation methods and a multiple regression model were tested.

Multiple polynomial regression is often used for the calculation of Hansen parameters from experimental solubilities of the test substance in a series of solvents with known parameters.[36,37] Because quadratic regression did not fit the data sufficiently, a fourth power model was applied for regressing the polymer swelling against the partial solubility parameters of the solvents used. The following equation was calculated:

$$\begin{aligned} y = {} & 929.8952 + 0.0095 \cdot \delta_d^4 - 0.6817 \cdot \delta_d^3 + 18.1386 \cdot \delta_d^2 \\ & - 212.7941 \cdot \delta_d - 9.07 \cdot 10^{-5} \cdot \delta_p^4 + 0.0020 \cdot \delta_p^3 \\ & - 0.0121 \cdot \delta_p^2 + 0.1634 \cdot \delta_p - 1.04 \cdot 10^{-4} \cdot \delta_h^4 \\ & + 0.0050 \cdot \delta_h^3 - 0.0759 \cdot \delta_h^2 + 0.3090 \cdot \delta_h \end{aligned} \quad (4)$$

where y is the polymer swelling and δ_d, δ_p, and δ_h are the Hansen solubility parameters of the solvents. Figure 3 shows a plot of this model. Although frequently used to define large-scale trends and patterns in datasets, polynomial regression is not really an interpolator because its primary aim is not the prediction of unknown values of a dependent variable.

The modified Shepard's method uses an inverse distance-weighted least-squares interpolation, whereas the nearest neighbor method assigns the value of the nearest data point to each grid node.[38,39] Both methods behave as exact interpolators, and this means that irregularly arranged data points are not smoothed but are always exactly honored.[40] The modified Shepard's method was chosen because it proved to be more suitable for irregularly spaced data and generated stepless contours (Fig. 3).

The method is based on the principle that each data point within a certain radius has some local influence on the value at the prediction location that diminishes with distance according to the following interpolation function $F(x, y, z)$:

$$F(x,y,z) = \sum_{k=1}^{N} W_k(x,y,z)\, Q_k(x,y,z) / \sum_{i=1}^{N} W_i(x,y,z) \quad (5)$$

where N is the number of data points. Q_k is a trivariate quadratic function that fits the values on a set of nearby nodes in a weighted least-squares sense and is defined by

$$\begin{aligned} Q_k(x,y,z) = {} & f_k + a_{k2}(x - x_k) + a_{k3}(y - y_k) + a_{k4}(z - z_k) \\ & + a_{k5}(x - x_k)(y - y_k) + a_{k6}(x - x_k)(z - z_k) \\ & + a_{k7}(y - y_k)(z - z_k) + a_{k8}(x - x_k)^2 \\ & + a_{k9}(y - y_k)^2 + a_{k10}(z - z_k)^2 \end{aligned} \quad (6)$$

with the coefficients f_k to a_{k10}. W_k and W_i are the weight functions assigned to each data point. The relative weights are defined by the inverse distance functions:

$$W_k(x,y,z) = \left[\frac{(R_\omega - d_k)_+}{R_\omega d_k} \right]^2 \quad (7a)$$

$$(R_\omega - d_k)_+ = \begin{cases} R_\omega - d_k & \text{if } d_k < R_\omega \\ 0 & \text{if } d_k \geq R_\omega \end{cases} \quad (7b)$$

where d_k is the Euclidean distance between the scatter point (x, y, z) and the interpolation point (x_k, y_k, z_k) and R_ω is a radius of influence about (x_k, y_k, z_k). The radius is chosen to be just large enough to include a fixed number of nodes.

The calculated interval volume encloses all points for which the effect parameter (e.g., the swelling degree) lies between a specified lower limit and the highest value of the data in the diagram. It has to be emphasized that the cutoff values determining the boundaries of the interval volumes are chosen arbitrarily for the best visualization of the distribution characteristics.

Influence of the polymer structure on the solubility

Figure 4 shows that each structure fragment of the polymer contributes to the shape of the volume, but even more latent structure information can be derived. For example, in the case of polyEDMA, the region of high swellability (the dark gray interval volume shown later in Fig. 7) covers unpolar solvents with high δ_d values, whereas the corresponding region of the EDMA/MAA copolymer (the dark gray interval volume shown later in Fig. 6 and the interval volume in Fig. 4) is shifted to lower δ_d values. In both cases, these regions of the interval volume adjacent to the δ_d axis represent the backbone

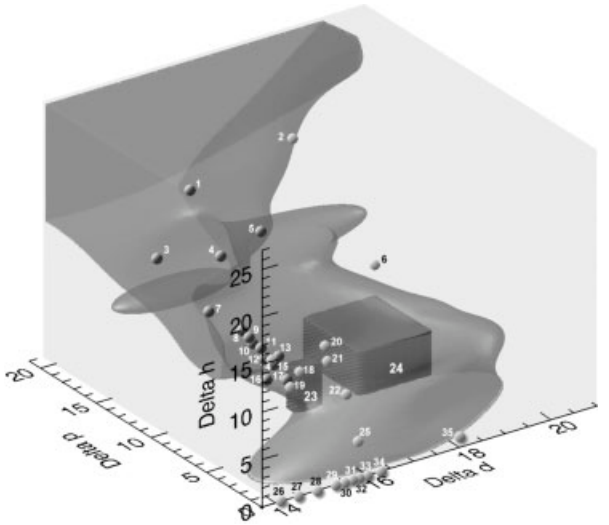

Figure 4 Three-dimensional representation of poly (EDMA-*co*-MAA) swelling in terms of the Hansen parameters ($MPa^{1/2}$). The interval volume encloses all solvents causing polymer swelling greater than or equal to 1.7%. The coordinates of substances that represent structure fragments of the polymer are marked with spheres (exactly defined coordinates of low-molecular-weight substances) and cubes (coordinate regions of polymers): (1) methanol, (2) ethylene glycol, (3) formic acid, (4) hydroxyethyl acrylate, (5) ethanol, (6) acrylic acid, (7) acetic acid, (8) methyl formate, (9) propionic acid, (10) ethyl formate, (11) methyl acrylate, (12) methyl acetate, (13) ethyl methacrylate, (14) butyric acid, (15) methyl propionate, (16) ethyl acrylate, (17) methyl methacrylate, (18) ethyl acetate, (19) octanoic acid, (20) ethylene glycol diacetate, (21) MAA, (22) stearic acid, (23) poly(ethyl methacrylate), (24) poly(methyl methacrylate), (25) polyethylene, (26) butane, (27) pentane, (28) hexane, (29) heptane, (30) octane, (31) decane, (32) nonane, (33) dodecane, (34) hexadecane, and (35) polypropylene.

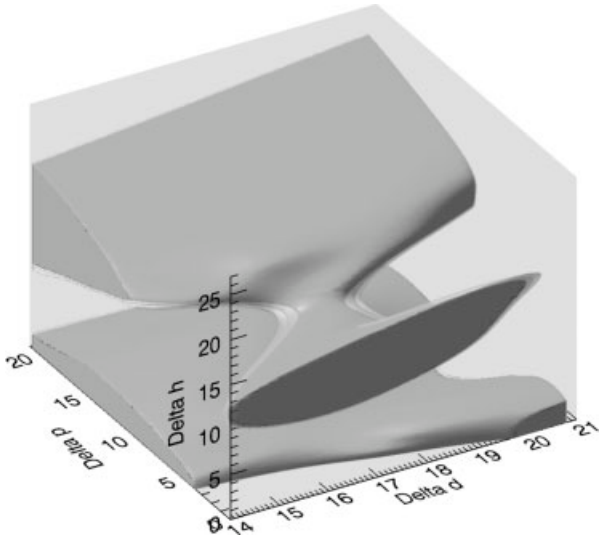

Figure 5 Three-dimensional representation of the specific surface area of poly(EDMA-*co*-MAA) samples in terms of the Hansen parameters ($MPa^{1/2}$). The interval volume encloses all porogens causing polymers with specific surface areas greater than or equal to 375 m^2/g (gray). The upper and lower limits of the 95% confidence interval are displayed as light gray and dark gray isosurfaces.

of the polymer chain. Scheduled data from the literature show that the solubility parameters of pure hydrocarbons ($\delta_p = \delta_h = 0$) are represented by data points on this axis.[34] δ_d rises with increasing molecular weight, and in the case of compounds with the same number of carbon atoms, it increases with decreasing molecular volume. This means that an interval volume bordering on the upper part of the δ_d axis, such as that in the case of polyEDMA, can be caused by long carbon chain fragments within the crosslinked polymer or by a dense structure due to a high degree of crosslinking.

Effects of the variations in the polymer–solvent affinity

Interval volumes displaying the distribution of the specific surface area of porous polymers prepared with different porogens were calculated in a similar way. Error calculations have been performed to display the precision of the method. Figure 5 shows an interval volume representing polymers with specific surface areas greater than or equal to 375 m^2/g. The upper and lower limits of the 95% confidence interval are displayed as isosurfaces in an onion-skin-like arrangement. Because the polymerization process, which determines the polymer structure, was performed at 60°C, a potential temperature dependence of solubility parameters should be considered. Although very limited attempts have been made so far to calculate solubility parameters at higher tem-

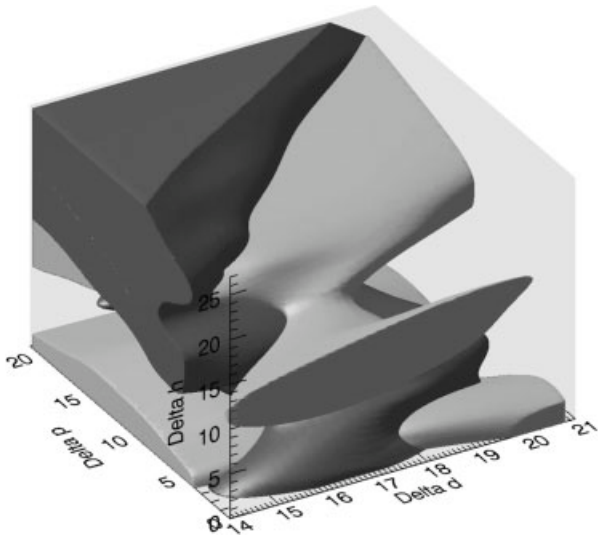

Figure 6 Three-dimensional representation of the poly (EDMA-*co*-MAA) swelling and specific surface area in terms of the Hansen parameters ($MPa^{1/2}$). Dark gray indicates solvents causing polymer swelling greater than or equal to 1.7%; light gray indicates porogens causing specific surface areas greater than or equal to 375 m^2/g.

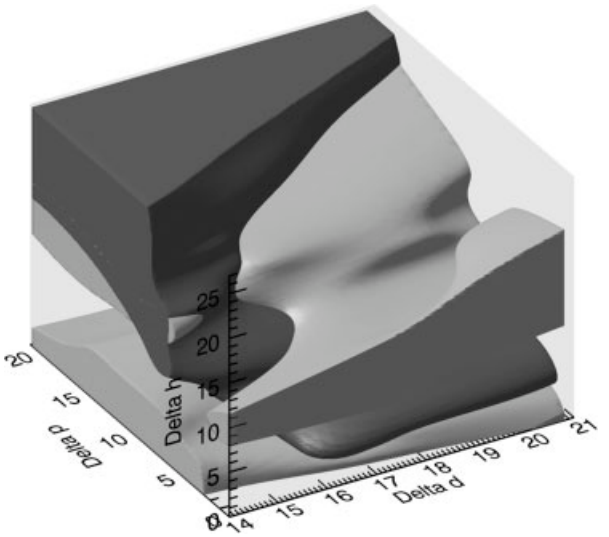

Figure 7 Three-dimensional representation of the poly-EDMA swelling and specific surface areas in terms of the Hansen parameters ($MPa^{1/2}$). Dark gray indicates solvents causing polymer swelling greater than or equal to 1%; light gray indicates porogens causing specific surface areas greater than or equal to 480 m^2/g.

peratures, the solubility parameter correlations of phenomena at higher temperatures have generally been found satisfactory when the parameters established at 25°C have been used.[34]

The superimposition of both models, that is, the swelling and surface area (Figs. 6 and 7), shows largely complementary volume shapes indicating that highly porous samples were obtained with solvents having low affinities to the polymer. As discussed before, this can be explained by early phase separation in poor solvents leading to smaller polymerization nuclei.

When the dark gray range is enlarged by the cut-off value being decreased from a swelling degree of 1.7% to a swelling degree of 0.01%, only those parts of the diagram remain unfilled that represent solvents with the lowest affinities to the polymer (Fig. 8). These ranges are largely congruent with the light gray marked regions indicating polymers with the greatest surface areas. Under this precondition of very poor solvation, the forming polymer chains undergo phase separation in an early stage of polymerization, leading to small nuclei with a densely packed structure. This prevents further infiltration of monomers and a secondary swelling process.

Contrary to the aforementioned conclusion, the diagram shows some regions in which dark gray volume segments, representing high solvent/polymer affinities, are overlapping with light gray shapes, indicating large surface areas. To understand this discrepancy, the properties of the initiator AIBN have to be considered. In the case of high affinity between the polymer and solvent, highly porous structures are formed only if the solvent additionally has good solubility for the initiator (overlapping segments of dark gray, light gray, and black volumes). Because of the distribution of the initiator, polymerization takes place mainly in the solution, outside of already formed nuclei, starting the concurrent growth of many polymer chains and subsequently generating a high number of small particles. This

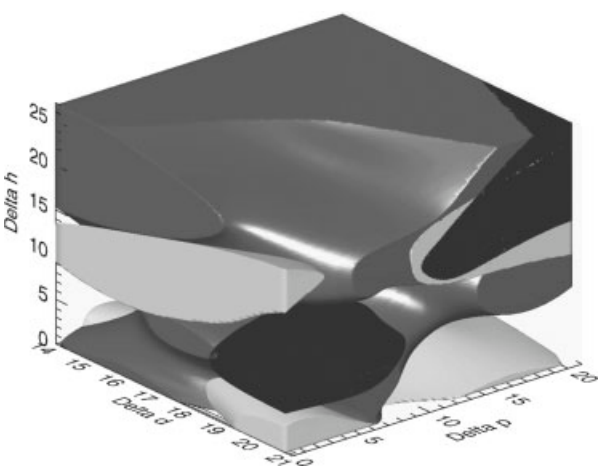

Figure 8 Three-dimensional representation of the poly (EDMA-*co*-MAA) swelling, specific surface area, and solubility of AIBN in terms of the Hansen parameters ($MPa^{1/2}$). Dark gray indicates solvents causing polymer swelling greater than or equal to 0.01%, light gray indicates porogens causing specific surface areas greater than or equal to 350 m^2/g, and black indicates solubility of AIBN greater than or equal to 0.99 (score).

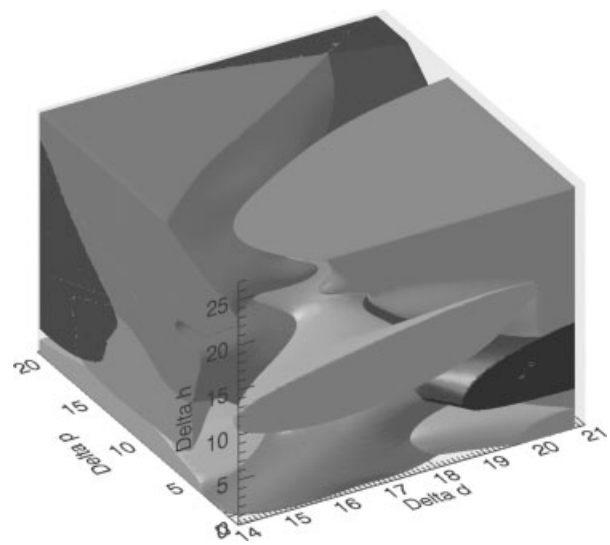

Figure 9 Three-dimensional representation of the poly (EDMA-*co*-MAA) swelling, specific surface area, and unreacted double bonds in terms of the Hansen parameters ($MPa^{1/2}$). Dark gray indicates solvents causing polymer swelling greater than or equal to 1.45%, light gray indicates porogens causing specific surface areas greater than or equal to 375 m^2/g, and medium gray indicates C=C/C=O IR signal ratios greater than or equal to 35.

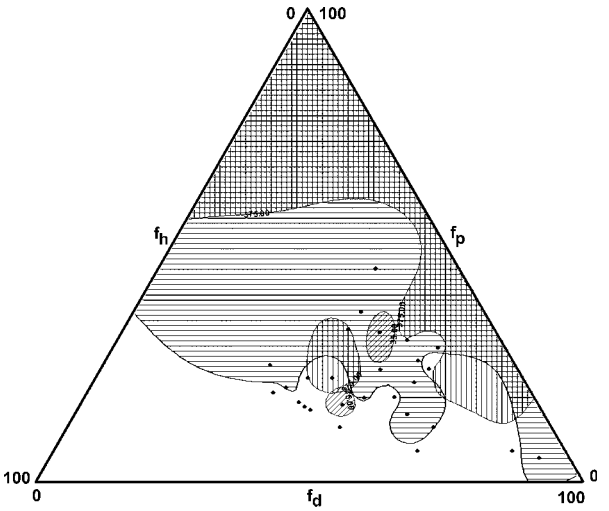

Figure 10 Data from Figure 9 presented as a triangular fractional Hansen parameter diagram (Teas plot) representing (≡) poly(EDMA-*co*-MAA) swelling greater than or equal to 1.45%, (| | |)specific surface areas greater than or equal to 375 m^2/g, and (///)C=C/C=O IR signal ratios greater than or equal to 35.

accounts for a rapid consumption of monomers that prevents both subsequent swelling of the nuclei and occlusive polymerization within the pores of their clusters.

On the other hand, solvents combining a high affinity to the polymer with a low solubility for the initiator cause the growth of long polymer chains. Phase separation occurs in a later stage of polymerization, leading to larger nuclei. The initiator migrates into the gel-like particles, at least into their surface layers, promoting secondary growth and the occlusion of voids between aggregated nuclei. As a result, structures with low surface areas are formed. In Figure 8, those solvents are located within all regions of the diagram in which the dark gray interval volumes (high polymer swelling) are not superimposed by black ones (high initiator solubility).

Saturation of double bonds

Figure 9 shows all diagram positions mapped in medium gray at which the solvent properties lead to a high quantity of unreacted double bonds in the formed polymer, which can be attributed to sterical hindrance of polymerization. The medium gray interval volume covers only those solvents causing medium polymer swelling but excludes those solvents with the highest and lowest affinities to the polymer.

In the case of high affinities to the solvent and consequently later phase separation, the unfolded structures of the growing polymer chains allow largely free accessibility for monomer molecules, which results in a high degree of conversion and low quantities of residual double bonds. If, on the other hand, densely packed nuclei are formed because of a lower polymer–solvent affinity, their core regions become sterically protected in an early state, and the polymerization remains incomplete. This should be expected also for the light gray ranges in the diagram marking samples with the highest surface areas. However, in this case, the formed globules are small enough that their core volumes are insignificant compared with their accessible surfaces, leading to a higher overall consumption rate of free binding sites. Assuming a regular spherical shape of the polymer forming subunits and a polymer density of 1.2 g/mL, it can be shown by a simple geometric calculation that a surface area of 375 m^2/g is attributable to a globule size of about 14 nm:

$$r = \frac{3}{\frac{S}{m} \cdot \rho} \tag{8}$$

where r is the radius of the globules, S/m is the specific surface area, and ρ is the density.

Provided that the thickness of the outermost globule layer is defined by the length of a repetitive unit of the polymer chain (0.24 nm), the volume of this layer amounts to at least 10% of the total volume if the globule diameter is 14 nm or less, and this means that at least 10% of the double bonds are accessible even if the core structure is densely packed and impermeable. By contrast, for samples with 38 (propylene glycol) or 4 m^2/g (hexane), the ratio of accessible double bonds is calculated to be only 1 or

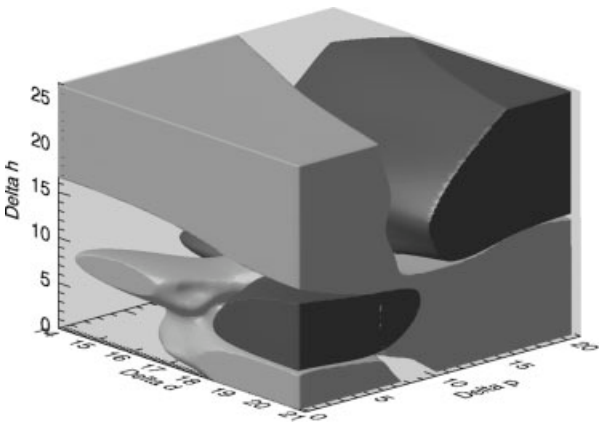

Figure 11 Three-dimensional representation of the microporosity of poly(EDMA-*co*-MAA) and solubility of AIBN in terms of the Hansen parameters ($MPa^{1/2}$). Gray indicates porogens causing a percentage of the micropore surface with respect to the total pore surface greater than or equal to 27%; black indicates solubility of AIBN greater than or equal to 0.99 (score).

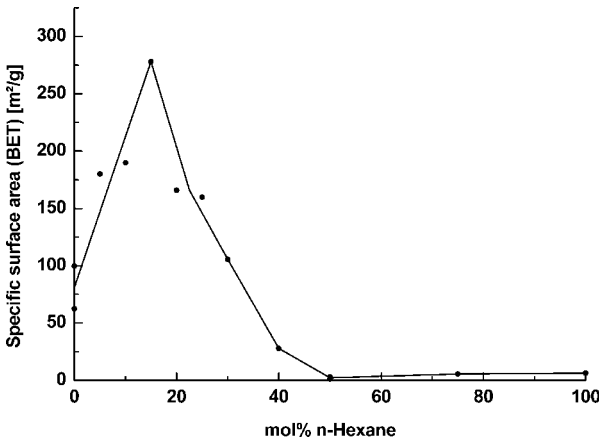

Figure 12 Specific surface area of polymer samples produced with different methanol/hexane mixtures versus the molar fraction of *n*-hexane.

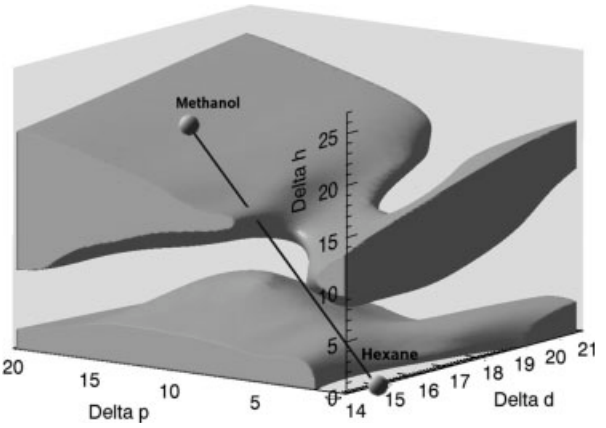

Figure 13 Three-dimensional representation of the specific surface area of poly(EDMA-*co*-MAA) samples in terms of the Hansen parameters ($MPa^{1/2}$). The interval volume encloses all porogens causing polymers with specific surface areas greater than or equal to 350 m^2/g. The coordinates of methanol/hexane mixtures are located on the connection line.

0.1%, respectively, resulting in a higher number of unreacted double bonds.

The final result of both counteracting effects—monomer access due to late phase separation or due to early phase separation followed by the formation of very small nuclei—is that sterical hindrance of polymerization particularly occurs in solvents with intermediate affinities to the polymer.

Figure 9 reveals a clear superiority of the presented three-dimensional graphic data analysis over the conventional Teas plot (Fig. 10), which is not able to visualize the mentioned correlations.

Ratio of the microporosity

The micropore and total pore surface areas can be separately determined by a *t*-plot analysis of the nitrogen adsorption data. Their ratio characterizes the contribution of micropores (<2 nm) to the overall porosity of the material. As shown in Figure 11, larger numbers of micropores are formed almost exclusively by those solvents that have comparatively low solubilities for the initiator. In those poor solvents, the initiator migrates into the surface layers of the polymer nuclei, promoting further polymerization and growth. As a result, the interparticular voids are shrunken, and mesopores (2–50 nm) are converted into micropores.

Solvent mixtures

The validity of the outlined method can also be proved for solvent mixtures. Figure 12 shows the specific surface areas of EDMA/MAA copolymers prepared with different methanol/hexane mixtures ranging from pure methanol to pure hexane. A maximum was found at a ratio of 85 mol % methanol and 15 mol % hexane, which was equivalent to 64 vol % methanol and 36 vol % hexane. The solubility parameter of a mixture ($\delta_{mixture}$) is the weighted average of its components:

$$\delta_{mixture} = \sum \Phi_i \delta_i \tag{9}$$

where Φ_i and δ_i are the volume fraction and solubility parameter of component i, respectively.[19] Thus,

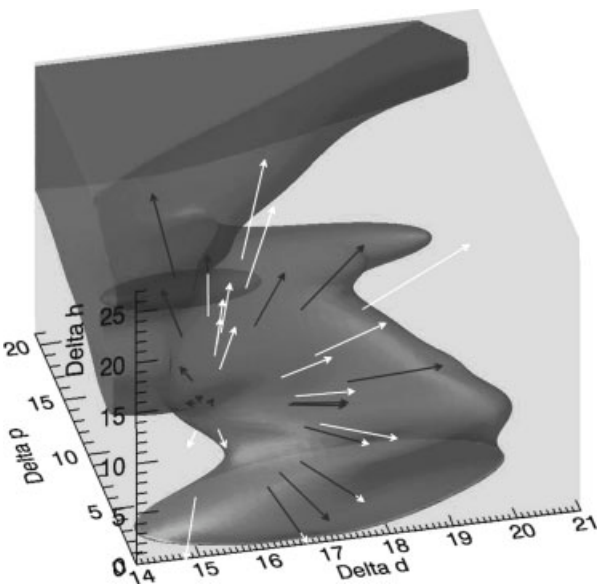

Figure 14 Three-dimensional representation of poly (EDMA-*co*-MAA) swelling (greater than or equal to 1.7%) in terms of the Hansen parameters ($MPa^{1/2}$). The arrows depict the shifting solubility parameters of the monomer–porogen mixtures during polymerization. Arrow positions inside the volume are colored black, and outer positions are colored gray.

the coordinates of a binary mixture are located on the connecting line between the coordinates of both components at a point corresponding in distance to their volume ratio. As shown in Figure 13, the intersection point with the interval volume divides the connecting line between methanol and hexane in the experimentally found 64 : 36 ratio mentioned previously.

It should be considered that the composition of the reaction mixture changes during polymerization. Monomers are consumed, and finally only the porogen remains as the liquid component. This causes a shift of the overall solubility parameter of the monomer–porogen mixture, which is depicted by the arrows in Figure 14 for each of the 30 solvents applied. For the computation of these arrows, the Hansen solubility parameters of EDMA were calculated according to the methods of Hoftyzer and van Krevelen and Hoy and aligned with the parameters of methyl methacrylate, which represents half a molecule of EDMA.[41] All other parameters are data from the literature. In some cases, the affinity of the polymer to the changing mixture decreases during the polymerization, whereas in other cases, it increases. This is one reason for often observed structural inhomogeneities within the polymer monoliths.

CONCLUSIONS

On the basis of a limited number of sample values, the developed method allows precise calculations of a variety of polymer properties for each solvent or solvent mixture defined by its Hansen solubility parameters. Because of the computation of a gridded data structure, mathematical analyses and statistical calculations are possible. Comparative three-dimensional mappings of the polymer swelling, surface area, microporosity, quantity of residual double bonds, and initiator solubility provide valuable information about the formation process of polymer microstructures. An important finding not described in the literature so far is the crucial role of the initiator solubility, which is a key element for the explanation of many contradictory solvent effects. It has to be stressed that most of the dependences between the analyzed parameters cannot be detected from raw data without graphic visualization.

Once developed for the coating industry and for predicting the compatibilities of polymers, Hansen solubility parameters have emerged as a versatile tool also in many other fields of application such as chromatography, extraction technology, and drug absorption studies. The presented computation method has the potential to provide significant benefits in all these areas.

References

1. Svec, F. Science 1996, 273, 205.
2. Horák, D.; Dvořák, P.; Hampl, A.; Šlouf, M. J Appl Polym Sci 2003, 87, 425.
3. Peters, E. C.; Svec, F.; Fréchet, J. M. J. Adv Mater 1999, 11, 1169.
4. Svec, F.; Fréchet, J. M. J. Ind Eng Chem Res 1999, 38, 34.
5. Guyot, A.; Bartholin, M. Prog Polym Sci 1982, 8, 277.
6. Seidl, J.; Malinský, J.; Dušek, K.; Heitz, W. Adv Polym Sci 1967, 5, 113.
7. Kun, K. A.; Kunin, R. J Polym Sci A-1: Polym Chem 1968, 6, 2689.
8. Okay, O. Prog Polym Sci 2000, 25, 711.
9. Bahar, I. Macromolecules 1987, 20, 1353.
10. Okay, O. J Appl Polym Sci 1999, 74, 2181.
11. Malik, M. A.; Ahmed, M.; Ikram, M. Polym Test 2004, 23, 835.
12. Malik, M. A.; Ali, S. W.; Waseem, S. J Appl Polym Sci 2006, 99, 3565.
13. Hamid, M. A.; Naheed, R.; Fuzail, M.; Rehman, E. Eur Polym J 1999, 35, 1799.
14. Svec, F.; Fréchet, J. M. J. Chem Mater 1995, 7, 707.
15. Viklund, C.; Svec, F.; Fréchet, J. M. J. Chem Mater 1996, 8, 744.
16. Xie, S.; Svec, F.; Fréchet, J. M. J. J Polym Sci Part A: Polym Chem 1997, 35, 1013.
17. Deleuzel, H.; Schultze, X.; Sherrington, D. C. Polym Bull 2000, 44, 179.
18. Shimn, S. E.; Oh, S.; Chang, Y. H.; Jin, M.-J.; Choe, S. Polymer 2004, 45, 4731.
19. Wernick, D. L. Ind Eng Chem Prod Res Dev 1984, 23, 240.
20. Van de Mark, M. R.; Lian, N. D. Polym Prepr 1987, 28, 160.
21. Ryu, J. H.; Kim, J. W.; Suh, K. D. Colloid Polym Sci 1999, 277, 1205.
22. Hattori, M.; Sudol, E. D.; El-Aasser, M. S. J Appl Polym Sci 1993, 50, 2027.
23. Barton, A. F. M. CRC Handbook of Solubility Parameters and Other Cohesion Parameters; CRC: Boca Raton, FL, 1991.
24. Hildebrand, J. H.; Scott, R. L. The Solubility of Nonelectrolytes; Dover: New York, 1964.
25. Hansen, C. M. J Paint Technol 1967, 39, 505.
26. Beerbower, A.; Dickey, J. R. ASLE Trans 1969, 12, 1.
27. Hansen, C. M. J Paint Technol 1967, 39, 104.
28. Hansen, C. M. Ind Eng Chem Prod Res Dev 1969, 8, 2.
29. Crowley, J. D.; Teague, G. S., Jr.; Lowe, J. W. J Paint Technol 1966, 38, 269.
30. Crowley, J. D.; Teague, G. S., Jr.; Lowe, J. W. J Paint Technol 1967, 39, 19.
31. Blanks, R. F.; Prausnitz, J. M. I & E Chem Fundam 1964, 3, 1.
32. Bagley, E. B.; Nelson, T. P.; Scigliano, J. M. J Paint Technol 1971, 43, 35.
33. Teas, J. P. J Paint Technol 1968, 40, 19.
34. Hansen, C. M. Hansen Solubility Parameters: A User's Handbook; CRC: Boca Raton, FL, 2000.
35. Nielson, G. M.; Sung, J. Proceedings of the 8th IEEE Visualization Conference, Phoenix, AZ, IEEE Computer Society Press: California, 1997, pp 221–228.
36. Bustamante, P.; Escalera, B.; Martin, A.; Selles, E. J Pharm Pharmacol 1993, 45, 253.
37. Verheyen, S.; Augustijns, P.; Kinget, R.; Van de Mooter, G. Int J Pharm 2001, 228, 199.
38. Renka, R. J. ACM Trans Math Software 1988, 14, 139.
39. Alfeld, P. In Mathematical Methods in Computer Aided Geometric Design; Lyche, T.; Schumaker, L., Eds.; Academic: New York, 1989.
40. Yang, C. S.; Kao, S. P.; Lee, F. B.; Hung, P. S. Proceedings of the XXth International Congress of ISPRS, Istanbul, Turkey, IAPRS XXXV/B2, pp 778–785.
41. Van Krevelen, D. W. Properties of Polymers: Their Correlation with Chemical Structure, Their Numerical Estimation and Prediction from Additive Group Contributions; Elsevier: Amsterdam, 1990.